Bounds on poloidal kinetic energy in plane layer convection

A. Tilgner
Institute of Geophysics, University of Göttingen, Friedrich-Hund-Platz 1, 37077 Göttingen, Germany
(Received 6 November 2017; published 21 December 2017)

A numerical method is presented that conveniently computes upper bounds on heat transport and poloidal energy in plane layer convection for infinite and finite Prandtl numbers. The bounds obtained for the heat transport coincide with earlier results. These bounds imply upper bounds for the poloidal energy, which follow directly from the definitions of dissipation and energy. The same constraints used for computing upper bounds on the heat transport lead to improved bounds for the poloidal energy.

DOI: 10.1103/PhysRevFluids.2.123502

I. INTRODUCTION

Transport in turbulent flows, for instance, heat flow across a turbulent convecting layer, cannot be computed analytically but has to be computed numerically or measured experimentally. However, rigorous analytical calculations can provide us with upper bounds on the transport. The oldest work finding upper bounds on turbulent dissipation seems to go back to Hopf [1]. Bounds for turbulent heat transport (which can also be expressed in terms of dissipation) appeared later in different forms. A series of papers including Refs. [2–4] leads to one method for obtaining upper bounds, called MHB method for short in this paper, and Constantin and Doering presented another method closely related to Hopf's original work [5,6] denoted as CDH method in the sequel. These two methods yield identical bounds if the best bounds obtainable within each method are compared. More recently, Seis [7] came up with another approach which obtains bounds from a very compact derivation.

The quality of the bounds obtained from the CDH method depends on the choice of a certain function, usually called background field. The optimal background field yielding the lowest upper bounds has again to be determined numerically. A direct computation from the Euler-Lagrange equations (as, for instance, in Ref. [8] for infinite Prandtl number convection) is cumbersome, which has prompted several authors [9–11] to search for alternatives. This paper presents yet another alternative. It employs the same constraints on the turbulent flow derived from the Navier-Stokes equation as previous methods but uses a reformulation which allows to numerically find the optimal background field through the solution of a semidefinite program (SDP), which is simpler to implement than the SDP directly derived from the CDH method solved in Ref. [11].

Apart from these technical issues, the main purpose of this paper is to explore the possibility of obtaining interesting bounds on energies. Previous work on bounds focused on dissipation or transport, but other properties are of interest as well. A bound on dissipation implies a bound on energy set by the maximal amount of energy that can exist in the least dissipative flow mode without violating the bound on dissipation. This argument is only based on the definitions of energy and dissipation and does not take into account that the flow field has to obey the Navier-Stokes equation. It is therefore of interest to see whether the constraints used in deriving bounds on dissipation can lead to improved bounds on energies. Since the expression for energy contains fewer derivatives and is less singular than the dissipation, one can hope that it is in some way simpler to find tight bounds on energies.

Section II starts with a precise statement of the problem. The general idea of the employed method is worked out in Sec. III taking as example upper bounds for the heat transport in infinite Prandtl number convection. The results are extended to general Prandtl number in Sec. IV. Section V finally presents bounds on the poloidal energy.

II. STATEMENT OF THE PROBLEM

Consider a plane layer of thickness h with bounding planes perpendicular to the z axis, infinitely extended in the x and y directions, and with gravitational acceleration acting in the direction of

negative z. The layer is filled with fluid of density ρ, kinematic viscosity ν, thermal diffusivity κ, and thermal expansion coefficient α. Top and bottom boundaries are held at the fixed temperatures $T_{\rm top}$ and $T_{\rm top}+\Delta T$, respectively. We will consider the equations of evolution immediately in nondimensional form, choosing for units of length, time, and temperature deviation from $T_{\rm top}$ the quantities h, h^2/κ, and ΔT. With this choice, the equations within the Boussinesq approximation for the fields of velocity $\boldsymbol{v}(\boldsymbol{r},t)$, temperature $T(\boldsymbol{r},t)$, and pressure $p(\boldsymbol{r},t)$ become

$$\frac{1}{\rm Pr}(\partial_t \boldsymbol{v}+\boldsymbol{v}\cdot\nabla\boldsymbol{v})=-\nabla p+{\rm Ra}\theta\hat{\boldsymbol{z}}+\nabla^2\boldsymbol{v}, \tag{1}$$

$$\partial_t\theta+\boldsymbol{v}\cdot\nabla\theta-v_z=\nabla^2\theta, \tag{2}$$

$$\nabla\cdot\boldsymbol{v}=0. \tag{3}$$

In these equations, $T=\theta+1-z$, so that θ represents the deviation from the conduction profile. The Prandtl number Pr and the Rayleigh number Ra are given by

$${\rm Pr}=\frac{\nu}{\kappa}\ ,\ {\rm Ra}=\frac{g\alpha\Delta T h^3}{\kappa\nu}, \tag{4}$$

and $\hat{\boldsymbol{z}}$ denotes the unit vector in z direction. The conditions at the boundaries $z=0$ and $z=1$ on the temperature are that $\theta=0$. Both stress free and no slip conditions will be investigated. At stress free boundaries, $\partial_z v_x=\partial_z v_y=v_z=0$, whereas $\boldsymbol{v}=0$ on no-slip boundaries.

It is convenient to decompose $\boldsymbol{v}$ into poloidal and toroidal scalars ϕ and ψ so that $\boldsymbol{v}=\nabla\times\nabla\times(\phi\hat{\boldsymbol{z}})+\nabla\times(\psi\hat{\boldsymbol{z}})$, which automatically fulfills $\nabla\cdot\boldsymbol{v}=0$. The z component of the curl and the z component of the curl of the curl of Eq. (1) yield the equations of evolution for ϕ and ψ,

$$\frac{1}{\rm Pr}(\partial_t\nabla^2\Delta_2\phi+\hat{\boldsymbol{z}}\cdot\nabla\times\nabla\times[(\nabla\times\boldsymbol{v})\times\boldsymbol{v}])=\nabla^2\nabla^2\Delta_2\phi-{\rm Ra}\Delta_2\theta, \tag{5}$$

$$\frac{1}{\rm Pr}(\partial_t\Delta_2\psi-\hat{\boldsymbol{z}}\cdot\nabla\times[(\nabla\times\boldsymbol{v})\times\boldsymbol{v}])=\nabla^2\Delta_2\psi, \tag{6}$$

with $\Delta_2=\partial_x^2+\partial_y^2$. For brevity, $\boldsymbol{v}$ is not replaced by its expression in terms of ϕ and ψ in these equations. The stress free boundary conditions translate into $\phi=\partial_z^2\phi=\partial_z\psi=0$ and the no slip boundary conditions become $\phi=\partial_z\phi=\psi=0$.

In the following, several types of averages will be important: the average over the entire volume, denoted by angular brackets without subscript, the average over an arbitrary plane $z=$ const., denoted by $\langle\ldots\rangle_A$, the average over a particular plane $z=z_0$, denoted by $\langle\ldots\rangle_{A,z=z_0}$, and the average over time, which will be signaled by an overline.

The dot product of $\boldsymbol{v}$ with Eq. (1), followed by a volume average, leads to

$$\partial_t\left\langle\frac{1}{2}\boldsymbol{v}^2\right\rangle=-{\rm PrRa}\langle\theta\Delta_2\phi\rangle-{\rm Pr}\langle|(\hat{\boldsymbol{z}}\times\nabla)\nabla^2\phi|^2+|\nabla\partial_x\psi|^2+|\nabla\partial_y\psi|^2\rangle. \tag{7}$$

Note that $v_z=-\Delta_2\phi$. Multiplication of Eq. (2) with θ and a subsequent volume average yields

$$\partial_t\left\langle\frac{1}{2}\theta^2\right\rangle=-\langle\theta\Delta_2\phi\rangle-\langle|\nabla\theta|^2\rangle. \tag{8}$$

The average of Eq. (2) over planes is noted for later reference:

$$\partial_t\langle\theta\rangle_A=\langle\partial_z(\theta\Delta_2\phi)\rangle_A+\left\langle\partial_z^2\theta\right\rangle_A. \tag{9}$$

We will seek below bounds on the Nusselt number Nu, defined as the time-averaged heat transport divided by the heat conducted if the fluid is at rest. ${\rm Nu}-1$ can be determined from the vertical derivative of θ averaged over top or bottom boundaries: ${\rm Nu}-1=-\langle\partial_z\overline{\theta}\rangle_{A,z=0}=-\langle\partial_z\overline{\theta}\rangle_{A,z=1}$. Integration of Eq. (9) from $z=0$ to any finite z, followed by time averaging, shows that $\langle\overline{\theta\Delta_2\phi}\rangle_A+\langle\partial_z\overline{\theta}\rangle_A$ is

identical at all height z, and in particular equal to $\langle \partial_z \overline{\theta} \rangle_{A,z=0}$ because $\Delta_2 \phi = 0$ at $z = 0$. An integration of $\langle \overline{\theta \Delta_2 \phi} \rangle_A + \langle \partial_z \overline{\theta} \rangle_A = \langle \partial_z \overline{\theta} \rangle_{A,z=0}$ over all z yields $\langle \overline{\theta \Delta_2 \phi} \rangle = \langle \partial_z \overline{\theta} \rangle_{A,z=0} = -\mathrm{Nu} + 1$, which yields an alternative expression for $\mathrm{Nu} - 1$, and by virtue of Eq. (8) one also has $\mathrm{Nu} - 1 = \langle \overline{|\nabla \theta|^2} \rangle$.

The second quantity for which we will seek bounds is the energy in the poloidal part of the velocity field, E_{pol}, given by

$$E_{\mathrm{pol}} = \left\langle \tfrac{1}{2} \overline{|\nabla \times \nabla \times (\phi \hat{\boldsymbol{z}})|^2} \right\rangle = \left\langle \tfrac{1}{2} \overline{|(\hat{\boldsymbol{z}} \times \nabla) \times \nabla \phi|^2} \right\rangle. \tag{10}$$

Because of the volume average, E_{pol} is strictly speaking an energy density.

Considerable simplification results in the limit of infinite Prandtl number. The time derivative and the advection term disappear from Eq. (1) in this limit. Equation (6) then implies that $\psi = 0$ and the momentum equation becomes a diagnostic equation for ϕ alone:

$$\nabla^2 \nabla^2 \Delta_2 \phi - \mathrm{Ra} \Delta_2 \theta = 0. \tag{11}$$

The temperature equation and the expressions for Nu and E_{pol} as well as the boundary conditions are not affected by setting Pr to infinity.

III. BOUNDS FOR CONVECTION AT INFINITE PRANDTL NUMBER

A. The method

This section explains the essence of the bounding method. Convection at infinite Prandtl number serves as a simple example for more general problems. The objective function Z defines the quantity for whose time average $\overline{Z}$ we wish to find a bound. For example, the choice $Z = \langle |\nabla \theta|^2 \rangle$ will yield bounds on $\overline{Z} = \mathrm{Nu} - 1$.

For infinite Pr, Eq. (11) allows us to eliminate ϕ in favor of θ and we are left with equations for θ only. The objective function Z also depends only on θ. Let us choose test functions $\varphi_n(z)$, $n = 1 \ldots N$, which depend on z only and project onto them the temperature Eq. (2):

$$\partial_t \langle \varphi_n \theta \rangle = \langle \varphi_n \partial_z (\theta \Delta_2 \phi) \rangle + \langle \varphi_n \nabla^2 \theta \rangle. \tag{12}$$

We now build a functional $G(\lambda_1 \ldots \lambda_N, \lambda_R, \theta)$ as a linear combination of the right hand sides of Eqs. (12) and (8):

$$G(\lambda_1 \ldots \lambda_N, \lambda_R, \theta) = \sum_{n=1}^{N} \lambda_n [\langle \varphi_n \partial_z (\theta \Delta_2 \phi) \rangle + \langle \varphi_n \nabla^2 \theta \rangle] + \lambda_R [\langle \theta \Delta_2 \phi \rangle + \langle |\nabla \theta|^2 \rangle]. \tag{13}$$

The variable ϕ has been left in the expression for G for better readability, but it does not appear as an argument of G because of Eq. (11) and $\Delta_2 \phi = \mathrm{Ra} (\nabla^2 \nabla^2)^{-1} \Delta_2 \theta$, where $(\nabla^2 \nabla^2)^{-1}$ is the inverse bi-Laplacian equipped with the boundary conditions for ϕ.

Assume that we know a set of coefficients $\lambda_1 \ldots \lambda_N, \lambda_R$ and an additional number λ_0 such that for our chosen objective function $Z(\theta)$ and all fields $\theta(\boldsymbol{r})$ obeying the boundary conditions for θ, the following inequality holds:

$$-Z + \lambda_0 + G(\lambda_1 \ldots \lambda_N, \lambda_R, \theta) \geqslant 0. \tag{14}$$

If this inequality is satisfied for every admissible θ, it is in particular satisfied by a solution of the equation of evolution. For such a solution and a set of λ's as specified above, we then have

$$0 = G - \sum_{n=1}^{N} \lambda_n \partial_t \langle \varphi_n \theta \rangle + \lambda_R \partial_t \left\langle \frac{1}{2} \theta^2 \right\rangle \geqslant Z - \lambda_0 + \partial_t \left[- \sum_{n=1}^{N} \langle \varphi_n \theta \rangle + \lambda_R \left\langle \frac{1}{2} \theta^2 \right\rangle \right]. \tag{15}$$

Taking the time average of the expression to the right of the inequality sign, we find $\overline{Z} \leqslant \lambda_0$. We see that we obtain an upper bound for $\overline{Z}$ as soon as we know a set of coefficients λ so that Eq. (14) is satisfied. The terms in G are at most quadratic in θ. If we wish to find upper bounds for dissipation or energy, Z is quadratic in θ, too. If θ is discretized, say, by spectral decomposition, the left-hand

side of inequality Eq. (14) is a quadratic form in the expansion coefficients of θ. Finding the sharpest bound on $\overline{Z}$ then amounts to minimizing λ_0 subject to the condition that the matrix appearing in the discretized form of inequality Eq. (14) be positive semidefinite. This problem has precisely the form of a semidefinite program.

To arrive at an implementable formulation, we have to select a discretization for θ and test functions φ_n. A decomposition into N Chebychev polynomials T_n for the z direction and into plane waves in x and y is chosen as a representation of θ:

$$\theta = \sum_{n=1}^{N} \sum_{k_x} \sum_{k_y} \hat{\theta}_{n,k_x,k_y} T_n(2z-1) e^{i(k_x x + k_y y)}. \tag{16}$$

The summation limits for k_x and k_y are not specified because they will turn out to be irrelevant. The coefficients $\hat{\theta}_{n,k_x,k_y}$ for any given k_x,k_y are not independent of each other because of the boundary conditions on θ at $z=0$ and $z=1$. Only N_f of the N coefficients are free. To enforce $\theta=0$ at $z=0$ and $z=1$, it is enough to set $N=N_f+2$. However, as reported below, it was found numerically advantageous to also explicitly enforce $\partial_z^2\theta=0$ at $z=0$ and $z=1$ [a relation which follows from Eq. (2) and all boundary conditions considered here], in which case $N=N_f+4$.

The test functions φ_n are chosen as delta functions centered at the collocation points in common use in time integration methods based on Chebychev discretization:

$$z_n = \frac{1}{2}\left[1+\cos\left(\pi\frac{n-1}{N-1}\right)\right], \quad n=1\ldots N \tag{17}$$

$$\varphi_n(z) = \delta(z-z_n). \tag{18}$$

Inserting all this into Eq. (14) leads to an inequality of the form

$$-\sum_{k_x,k_y} \boldsymbol{x}^*_{k_x,k_y} \boldsymbol{Z}_k \boldsymbol{x}_{k_x,k_y} + \lambda_0 + \sum_{n=1}^{N} \lambda_n \sum_{k_x,k_y} \boldsymbol{x}^*_{k_x,k_y} \boldsymbol{G}_{nk} \boldsymbol{x}_{k_x,k_y} + \boldsymbol{x}^*_{k_x,k_y} \lambda_R \boldsymbol{E}_k \boldsymbol{x}_{k_x,k_y} \geqslant 0. \tag{19}$$

The superscripted star denotes complex conjugation. The matrices $\boldsymbol{Z}_k$, $\boldsymbol{E}_k$, and $\boldsymbol{G}_{nk}$ are real. Their entries depend on k_x and k_y only in the combination $k^2=k_x^2+k_y^2$ and there are no terms coupling different k. Furthermore, these matrices are symmetric. The vectors $\boldsymbol{x}_{k_x,k_y}$ are constructed as $\boldsymbol{x}_{k_x,k_y} = (1,\hat{x}_{1,k_x,k_y},\hat{x}_{2,k_x,k_y},\ldots,\hat{x}_{N_f,k_x,k_y})$, where the $\hat{x}_{n,k_x,k_y}$ are linear combinations of the $\hat{\theta}_{n,k_x,k_y}$ in Eq. (16). They appear in an expansion analogous to Eq. (16) as the coefficients of N_f linear combinations of the first N Chebychev polynomials satisfying the boundary conditions. The 1 in the first component of $\boldsymbol{x}_{k_x,k_y}$ is necessary to accommodate the term linear in θ in the $k=0$ summand in Eq. (19). It also allows us to write λ_0 as $\sum_{k_x,k_y} \boldsymbol{x}^*_{k_x,k_y} \lambda_0 \boldsymbol{H}_k \boldsymbol{x}_{k_x,k_y}$ with $\boldsymbol{H}_k=0$ for $k\neq 0$ and all entries of $\boldsymbol{H}_0$ are zero except that $H_{0,1,1}=1$.

Inequality Eq. (19) therefore has the form

$$\sum_{k_x,k_y} \boldsymbol{x}^*_{k_x,k_y} \left[-\boldsymbol{Z}_k + \lambda_0 \boldsymbol{H}_k + \sum_{n=1}^{N} \lambda_n \boldsymbol{G}_{nk} + \lambda_R \boldsymbol{E}_k\right] \boldsymbol{x}_{k_x,k_y} \geqslant 0. \tag{20}$$

For λ_0 to serve as an upper bound, this inequality must be satisfied for all $\boldsymbol{x}_{k_x,k_y}$, which requires that $[-\boldsymbol{Z}_k + \lambda_0 \boldsymbol{H}_k + \sum_{n=1}^{N} \lambda_n \boldsymbol{G}_{nk} + \lambda_R \boldsymbol{E}_k]$ be positive semidefinite for all k. The SDP to be solved is in summary:

$$\begin{aligned} &\text{minimize } \lambda_0 \\ &\text{subject to } -\boldsymbol{Z}_k + \lambda_0 \boldsymbol{H}_k + \sum_{n=1}^{N} \lambda_n \boldsymbol{G}_{nk} + \lambda_R \boldsymbol{E}_k \succeq 0 \quad \text{for all } k, \end{aligned} \tag{21}$$

where $\boldsymbol{M} \succeq 0$ means that the matrix $\boldsymbol{M}$ is positive semidefinite.

The symmetry about the midplane can be exploited to alleviate the numerical task of solving the SDP. This symmetry suggests to construct linear combinations of the constraints Eq. (12) in the form of equations for $\partial_t(\langle\varphi_i\theta\rangle \pm \langle\varphi_{N+1-i}\theta\rangle), i = 1 \ldots N/2$. It turns out that only the equations with the minus sign constrain λ_0, the other equations are redundant. Symmetry affects also the parity of the most dangerous functions which most readily violate the inequality constraint of the SDP. Expanding θ in the functions $T_{n+2}(2z-1) - T_n(2z-1)$, which are by construction zero at $z = 0$ and $z = 1$, one only needs to retain odd n for $k = 0$ and even n for $k \neq 0$. The other combinations do not affect the best bound.

It may seem like a formidable task to enforce the inequality condition in Eq. (21) for all k. In fact, it is not. Barring any special symmetry or degeneracy in the matrices involved, the inequality will hold as a strict inequality for almost all k and as an equality only for a finite set of k, the active set in the parlance of optimization. The active set tends to be small. As an example, pretend that we are looking for a bound on dissipation so that $Z = \langle|\nabla\theta|^2\rangle$. We should be able to prove that dissipation is zero for Ra below onset. This requires $\lambda_0 = 0$. We can find a suitable set of coefficients by setting $\lambda_1 = \lambda_2 = \cdots = \lambda_N = 0$ and only $\lambda_R \neq 0$. Equation (14) becomes $\lambda_R\langle\theta\Delta_2\phi\rangle + (\lambda_R - 1)\langle|\nabla\theta|^2\rangle \geqslant 0$. The last term suggests that we are best off choosing λ_R positive and large compared with 1, so that the condition

$$\langle\theta\Delta_2\phi\rangle + \langle|\nabla\theta|^2\rangle \geqslant 0 \tag{22}$$

needs to be satisfied for all admissible θ [ϕ being determined by Eq. (11)]. The left-hand side of Eq. (22) is equal to $-\partial_t\langle\frac{1}{2}\theta^2\rangle$, so that Eq. (22) is nothing but the condition for energy stability. The θ which yields the largest possible left hand side is determined from a linear Euler-Lagrange equation with coefficients independent of k, since the left-hand side itself has no k dependent coefficients. The optimal θ has therefore a single Fourier component. At the critical Rayleigh number, the inequality condition in Eq. (21) is fulfilled with the equality sign for one value of k and as a strict inequality for all other k. At least at this Ra, the active set contains only one element. As Ra is increased, the active set gradually becomes larger, adding one element after the other.

All results presented in this paper were computed with an automated search for the active set. As one is usually interested in some bound as a function of Ra, start with a small Ra and a tentative active set of two elements: $k = 0$, which is always necessary for any $\lambda_i \neq 0, 1 \leqslant i \leqslant N$ because of the last term in Eq. (12), and an additional $k \neq 0$. Then run an optimization over the nonzero k which maximizes λ_0, where λ_0 is the result of the SDP problem

$$\begin{aligned} &\text{minimize } \lambda_0 \\ &\text{subject to } -\boldsymbol{Z}_k + \lambda_0\boldsymbol{H}_k + \sum_{n=1}^{N}\lambda_n\boldsymbol{G}_k + \lambda_R\boldsymbol{E}_k \succeq 0 \quad \text{for all } k \text{ in the active set.} \end{aligned} \tag{23}$$

This maximization selects the wave numbers k, which impose the most stringent constraint on λ_0. Once the maximum is found, it remains to check whether the active set is complete. For this purpose, the matrix $[-\boldsymbol{Z}_k + \lambda_0\boldsymbol{H}_k + \sum_{n=1}^{N}\lambda_n\boldsymbol{G}_{nk} + \lambda_R\boldsymbol{E}_k]$ is assembled for 1000 values of k regularly spaced on a logarithmic scale for k between 0.1 an 10^4, and for each matrix, a Cholesky decomposition is attempted. If the matrix is positive semidefinite at all tested wave numbers, the calculation advances to the next higher Ra to compute the next bound. If the Cholesky decomposition fails, one has found a k which violates the inequality constraint in the SDP. The tentative active set is then enlarged by one element and the maximization of λ_0 over the wave numbers in the active set is run anew. If the new maximal λ_0 is larger by at least 0.1% than the previous result, the new active set is accepted as such and Ra is increased to compute the next bound. If the fractional increase is less than 0.1%, the newly added k is rejected as a false alarm and the old active set is used as the starting point for the computation of the bound at the next Ra. This rejection is a useful procedure because tolerances in the optimization together with round off errors accumulated during the Cholesky decomposition may lead the method to spuriously signal a violation of the constraint of

positive semidefiniteness. The most straightforward way to distinguish a spurious from a warranted detection of violation is to check whether an enlarged set of wave numbers leads to a more stringent constraint on λ_0. If it does not, the enlargement was unnecessary.

The most time consuming step in this entire method is the solution of the SDP. This was done with the Python interfaced version of the package cvxopt available from cvxopt.org, using either the internal solver of cvxopt or dsdp5. These codes implement central path methods which have the reputation of being the best choice for small to medium size problems. Resolutions of up to $N = 512$ were used for the results presented in this paper which are limited in Rayleigh number not because of an overwhelming computational burden, but because the SDP solvers failed to converge at large Ra. The SDP package was used as a black box which precluded a precise tracking of the problem, but round-off issues are the most likely culprit. Ierley et al. [8] report that they had to use a 96-digit floating-point representation to cover their interval of Ra in an implementation of the CDH method. The package used for the present work did not allow one to vary floating point types, so that the effect of the data type on convergence was not tested. The internal solver of cvxopt allowed to treat slightly larger Ra than dsdp5, and if both methods converged, they converged to the same result.

Even though it is enough to enforce $\theta = 0$ at the boundaries, it helped to require $\partial_z^2\theta = 0$ as well. Again, both sets of boundary conditions lead to the same results if the SDP solver converges, but the extended boundary conditions allow one to reach higher Ra. The use of Chebychev polynomials is not the root of the convergence problems. For free-slip boundaries, it is also convenient to choose $\varphi_n = \sin(n\pi z)$ and an expansion of θ in $\sin(n\pi z)$ instead of Chebychev polynomials. This choice also leads to convergence problems at very much the same Ra.

Some relief is provided by an obvious modification of the method which consists in integrating by parts in Eq. (12) to obtain

$$\partial_t \langle \varphi_n \theta \rangle = -\langle (\partial_z \varphi_n)\theta \Delta_2 \phi \rangle - \langle (\partial_z \varphi_n)(\partial_z \theta) \rangle + \varphi_n(1)\langle \partial_z \theta \rangle_{A,z=1} - \varphi_n(0)\langle \partial_z \theta \rangle_{A,z=0} \tag{24}$$

and to choose the test functions φ_n such that $\partial_z \varphi_n = \delta(z - z_n)$ with the Chebychev collocation points defined in Eq. (17). To preserve the symmetry about $z = 1/2$, one can express the test function at the boundaries as

$$\begin{aligned} \varphi(0) &= \varphi\left(\frac{1}{2}\right) + \int_{\frac{1}{2}}^{0} \partial_z \varphi dz = \varphi\left(\frac{1}{2}\right) - \sum_{n=1}^{N/2} \lambda_n, \\ \varphi(1) &= \varphi\left(\frac{1}{2}\right) + \int_{\frac{1}{2}}^{1} \partial_z \varphi dz = \varphi\left(\frac{1}{2}\right) + \sum_{n=N/2+1}^{N} \lambda_n, \end{aligned} \tag{25}$$

for $\varphi(z) = \sum_{n=1}^{N} \lambda_n \varphi_n(z)$ with N even. We can therefore replace the functional G with G' defined as

$$\begin{aligned} G'(\lambda_1 \ldots \lambda_N, \lambda_R, \theta) = &- \sum_{n=1}^{N} \lambda_n \langle \delta(z - z_n)[\theta \Delta_2 \phi + \partial_z \theta] \rangle + \varphi\left(\frac{1}{2}\right)(\langle \partial_z \theta \rangle_{A,z=1} - \langle \partial_z \theta \rangle_{A,z=0}) \\ &+ \sum_{n=1}^{N/2} \lambda_n \langle \partial_z \theta \rangle_{A,z=0} + \sum_{n=N/2+1}^{N} \lambda_n \langle \partial_z \theta \rangle_{A,z=1} + \lambda_R[\langle \theta \Delta_2 \phi \rangle + \langle |\nabla \theta|^2 \rangle], \end{aligned} \tag{26}$$

and we must obtain identical results if we replace G with G' in Eq. (14). Because of the symmetry of the optimal test function, $\varphi(z) = -\varphi(1 - z)$ so that $\varphi(\frac{1}{2}) = 0$, and the second term in G' disappears. G' still looks more complicated than G but does not contain second derivatives. As a result, the implementation using G' has better convergence properties and is preferred for this reason.

Finally, rescaling λ_0 improves convergence. If the optimal λ_0 approximately equals $c\mathrm{Ra}^\gamma$ with some constants c and γ, it helps to use the variable $\lambda_0' = \lambda_0/(c\mathrm{Ra}^\gamma)$ instead of λ_0 itself as an argument of the functional G'.

The central path methods also solve the dual problem. This part of the output allows one to compute the derivative of the optimal λ_0 with respect to problem parameters such as the wave numbers k (see example 5.13 in Ref. [12]). This opens the possibility of using a gradient based method for maximizing λ_0 over k. This was done with a Newton-BFGS method. However, to run advantageously, this method needs derivatives with a higher precision than what the SDP solver sometimes provides. If the progress of Newton-BFGS was too slow, it was replaced by the gradient free Nelder-Mead optimization.

B. Relation with other methods

The background field or CDH method can be directly mapped onto the method of this section. It proceeds by using a different variable for the temperature variation, defined by $T(\boldsymbol{r},t) = \tau(z) + \theta'(\boldsymbol{r},t)$ where the background field τ is chosen such that $\tau(0) = 1$, $\tau(1) = 0$, and $\theta' = 0$ on the boundaries. It follows from the temperature Eq. (2) that

$$\partial_t \left\langle \frac{1}{2}\theta'^2 \right\rangle = -\langle \partial_z \theta' \partial_z \tau \rangle - \langle v_z \theta' \partial_z \tau \rangle - \langle |\nabla \theta'|^2 \rangle. \tag{27}$$

The CDH method now consists in finding $\tau(z)$, λ_0, and λ_R such that

$$-Z + \lambda_0 - \lambda_R(\langle \partial_z \theta' \partial_z \tau \rangle + \langle v_z \theta' \partial_z \tau \rangle + \langle |\nabla \theta'|^2 \rangle) \geqslant 0 \tag{28}$$

for all admissible θ' and v_z, in which case $\overline{Z} \leqslant \lambda_0$. This problem is not directly an SDP if τ appears quadratically in Z. It is then necessary to form a Schur complement to recover an optimization problem in SDP form [11]. This complicates a direct implementation of the CDH method compared with the method presented above. However, the bounds obtained from both methods must be identical, because after the identification $\varphi(z) = \sum \lambda_n \varphi_n(z) = \lambda_R(\tau - 1 + z)$ one recognizes Eqs. (28) and (14) to be the same. This also means that the boundary layer structure typical of optimal background fields will also appear in $\varphi(z)$, and we also see that φ obeys $\varphi(0) = \varphi(1) = 0$.

As a further variation of the bounding problem, and to make contact with ref. [7], consider the test function φ_S with $\varphi_S = 1$ for $z \leqslant l$ and $\varphi_S = 0$ for $l < z \leqslant 1$ for some l with $0 < l < 1$. We then obtain

$$\partial_t \langle \varphi_S \theta \rangle = -\int_0^l \langle \theta \Delta_2 \phi + \partial_z \theta \rangle_A dz - \langle \partial_z \theta \rangle_{A,z=0} \tag{29}$$

whose discretization is a suitable linear combination of Eq. (24). A bound for any time averaged Z in the form $\overline{Z} \leqslant \lambda_0$ is then obtained if one finds λ_0, l, and λ_R such that

$$-Z + \lambda_0 - \int_0^l \langle \theta \Delta_2 \phi + \partial_z \theta \rangle_A dz - \langle \partial_z \theta \rangle_{A,z=0} + \lambda_R[\langle \theta \Delta_2 \phi \rangle + \langle |\nabla \theta|^2 \rangle] \geqslant 0 \tag{30}$$

for all admissible θ and ϕ. Seis [7] further restricts the problem to $\lambda_R = 1$ and shows how to solve it for general Prandtl number.

The functional G contains a linear combination of expressions which are the right-hand sides of the time evolution equations of terms which are linear or quadratic in the flow variables θ, ϕ, ψ. One could add linear combinations of the right hand sides of time evolution equations for higher moments, which would be equivalent to the auxiliary function approach [13,14]. This leads to an optimization problem with a constraint of the form that some polynomial must always be positive. An SDP can then only be formulated after relaxing this constraint to the less restrictive requirement that this polynomial is a sum of squares [13,14].

C. Heat transport

We will now consider bounds on the heat transport as a validation of the method presented in this section. These bounds are obtained by setting $Z = \langle |\nabla \theta|^2 \rangle$, or $Z = \langle -\theta \Delta_2 \phi \rangle$ or $Z = \langle -\partial_z \theta \rangle_{A,z=0}$.

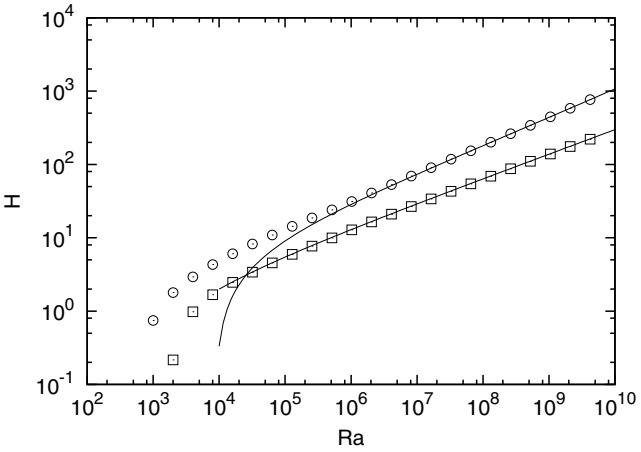

FIG. 1. The optimal upper bound H for the advective heat transport $\mathrm{Nu}-1$ as a function of Ra for stress free (circles) and no slip (squares) boundary conditions and infinite Pr. The continuous lines show formulas obtained from fits in Ref. [8], which are $H = 0.101 \times \mathrm{Ra}^{0.4} + 0.70965 \times \mathrm{Ra}^{0.2} - 7.166 - 1$ for free-slip boundaries and $H = 0.139 \times \mathrm{Ra}^{1/3} - 1$ for no slip boundaries.

With all these three choices, $\overline{Z} = \mathrm{Nu} - 1$, and the results obtained with the method described above are indeed the same. Figure 1 shows the optimal bound H on $\mathrm{Nu} - 1$ found for both stress free and no slip boundaries. The distinction between the two boundary conditions appears only in the boundary conditions for the inverse bi-Laplacian in Eq. (11).

For both boundary conditions, Ierley *et al.* [8] have obtained bounds from numerical optimization within the CDH method. Approximate expressions for those bounds are also included in Fig. 1. These bounds conform with the analytical result that $H \leqslant c_f \mathrm{Ra}^{5/12}$ for free-slip boundaries [15] with some constant c_f. Lower bounds are obtained if the number of elements in the active set is limited. The formula quoted in the caption of Fig. 1 is valid for up to two wave numbers in the active set, which is appropriate for the range of Ra in Fig. 1, and which is a more accurate fit than the universally valid bound proportional to $\mathrm{Ra}^{5/12}$. For no slip boundaries, it is known [16] that the CDH method cannot yield bounds better than proportional to $\mathrm{Ra}^{1/3}(\ln \mathrm{Ra})^{1/15}$. This agrees with the result of Ref. [8] apart from the virtually undetectable factor $(\ln \mathrm{Ra})^{1/15}$.

Bounds obtained from the MHB method can be found in Ref. [17] and in tabulated form in Vitanov's doctoral thesis [18]. The numbers in the thesis match the results shown in Fig. 1 to four digits accuracy.

Figure 2 shows the wave numbers included in the active set for the example of free-slip boundaries. These are not exactly the same as those given in the analogous Fig. 12(b) of Ref. [8], which shows an additional wave number at $\mathrm{Ra} > 10^9$. This difference simply comes from the tolerances set in the automated search of the wave numbers. The additional wave number for Ra above 10^9 does increase the bound H, but by less than 0.1% which is why it was rejected and does not appear in Fig. 2.

IV. BOUNDS ON HEAT TRANSPORT AT GENERAL PRANDTL NUMBER

For finite Pr, one has to return to the general Eqs. (5) and (6). The equations of evolution for $\langle\theta\rangle_A$ and $\langle\frac{1}{2}\theta^2\rangle$, Eqs. (9) and (8) remain unchanged, but the dot product of the momentum Eq. (1) with $\boldsymbol{v}$, averaged over the entire volume, now yields the additional non trivial information in Eq. (7) that

$$\partial_t \left\langle \frac{1}{2}\boldsymbol{v}^2 \right\rangle = -\mathrm{PrRa}\langle\theta\Delta_2\Phi\rangle - \mathrm{Pr}\langle|(\hat{\boldsymbol{z}}\times\nabla)\nabla^2\phi|^2\rangle - \mathrm{Pr}D_{\mathrm{np}} \tag{31}$$

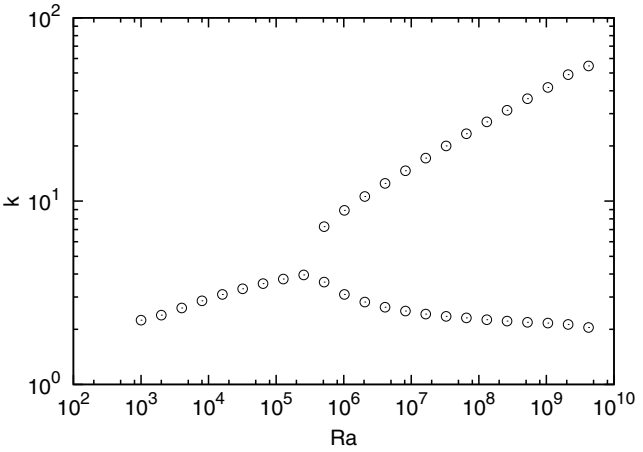

FIG. 2. Wave numbers k in the active set for the optimization of the bound H for free-slip boundary conditions and infinite Pr.

with the toroidal dissipation

$$D_{\mathrm{np}} = \langle |\nabla \partial_x \psi|^2 + |\nabla \partial_y \psi|^2 \rangle. \tag{32}$$

The subscript stands for nonpoloidal, because if periodic boundary conditions are imposed on ψ, this term has to include not only the dissipation due to the toroidal field but also the dissipation due to a horizontal mean flow [19]. Since $D_{\mathrm{np}} \geqslant 0$, it will be convenient to introduce a new variable d defined by $d^2 = D_{\mathrm{np}}$.

We can now follow the same line of thought as in the previous section and construct a functional F as

$$\begin{aligned} F(\lambda_1 \ldots \lambda_N, \lambda_R, \lambda_E, \theta, \phi, d) = \sum_{n=1}^{N} \lambda_n \left\langle \varphi_n \left[\partial_z (\theta \Delta_2 \phi) + \partial_z^2 \theta \right] \right\rangle + \lambda_R [\langle \theta \Delta_2 \phi \rangle + \langle |\nabla \theta|^2 \rangle] \\ + \lambda_E [\mathrm{Ra} \langle \theta \Delta_2 \phi \rangle + \langle |(\hat{\boldsymbol{z}} \times \nabla) \nabla^2 \phi|^2 \rangle] + \lambda_E d^2 \end{aligned} \tag{33}$$

and conclude that if we know $\lambda_0, \lambda_1 \ldots \lambda_N, \lambda_R, \lambda_E$ such that

$$-Z + \lambda_0 + F(\lambda_1 \ldots \lambda_N, \lambda_R, \lambda_E, \theta, \phi, d) \geqslant 0 \tag{34}$$

for all admissible θ, ϕ, and all d, we get the estimate $\overline{Z} \leqslant \lambda_0$. The functional F has to include both θ and ϕ as independent arguments because the relation Eq. (11) no longer holds for finite Pr. There is also an additional coefficient λ_E which has to be positive to satisfy the inequality Eq. (34) for all d.

The bounding method was numerically implemented for stress-free boundaries using identical expansions for θ and ϕ into Chebychev polynomials and Fourier series, and using the same test functions φ_n as for infinite Pr in the previous section. The optimizing fields θ and ϕ again have symmetry, which was exploited in the calculations with high resolutions. When expanded in $T_{n+2}(2z-1) - T_n(2z-1)$, the Fourier components of both θ and ϕ contain only terms with even n for $k > 0$. There is no contribution to ϕ with $k = 0$, and the zero wavenumber contribution to θ contains only terms with odd n. Expressed differently, if $\theta = \sum_{k_x,k_y} \tilde{\theta}_{k_x,k_y} e^{i(k_x x + k_y y)}$ and $k^2 = k_x^2 + k_y^2$, then $\tilde{\theta}_{k_x,k_y}(z) = \tilde{\theta}_{k_x,k_y}(1-z)$ and $\tilde{\theta}_{0,0}(z) = -\tilde{\theta}_{0,0}(1-z)$, and likewise for the poloidal field. The optimal $\varphi(z)$ has the same symmetry as for infinite Pr.

Bounds H for $\mathrm{Nu} - 1$ are obtained by setting Z to either of the following expressions: $\langle |\nabla \theta|^2 \rangle$, $\langle -\theta \Delta_2 \phi \rangle$, or $\langle -\partial_z \theta \rangle_{A, z=0}$. All three options yield identical results and they agree to four digits

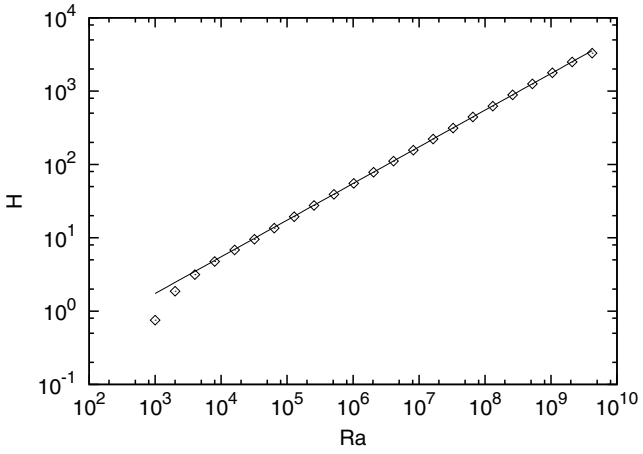

FIG. 3. The optimal upper bound H for the advective heat transport $\mathrm{Nu} - 1$ as a function of Ra for stress free boundaries and general Pr. The continuous line indicates the power law $0.055 \times \mathrm{Ra}^{1/2}$.

accuracy with values listed in Vitanov's thesis [18]. The result is shown in Fig. 3. The bounds obey approximately $H = 0.055 \times \mathrm{Ra}^{1/2}$. The active set now contains more wave numbers, as shown in Fig. 4.

V. BOUNDS ON THE VELOCITY FIELD

The previous sections investigated bounds on heat transport or thermal dissipation, a quantity obtainable from the temperature field alone. The present section deals with the velocity field, which is characterized first and foremost by its energy. Rewriting Eq. (7), the dissipation of the velocity field is given by

$$\sum_{ij} \langle \overline{(\partial_j v_i)^2} \rangle = \mathrm{Ra}(\mathrm{Nu} - 1), \tag{35}$$

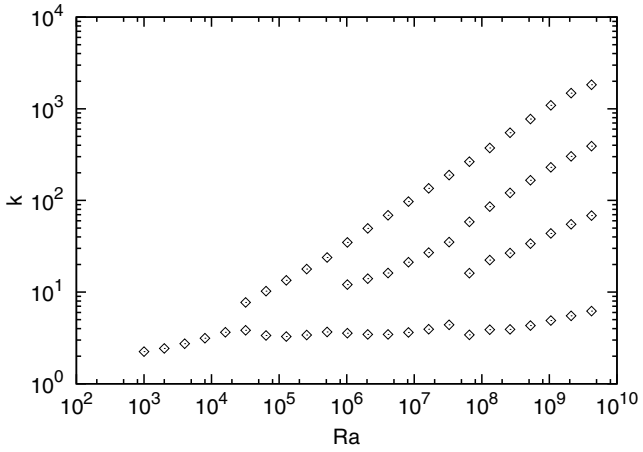

FIG. 4. Wave numbers k in the active set for the optimization of the bound H for free-slip boundary conditions and general Pr.

so that a bound on $\mathrm{Nu}-1$ also bounds the kinetic dissipation. We can now invoke Poincaré's inequality, which states that $\int_0^1(\partial_z f)^2dz \geqslant \eta\int_0^1 f^2dz$ for any function $f(z)$ defined on the interval $0\leqslant z\leqslant 1$, where η is the smallest eigenvalue of the Laplace equation $-\partial_z^2 g=\eta g$, if g and f obey the same boundary conditions. For Dirichlet boundaries, $\eta=\pi^2$. Neumann boundary conditions do not uniquely select a solution. If f obeys $\int_0^1 f(z)dz=0$ in addition to the Neumann conditions, one has again $\eta=\pi^2$. We now also use the fact that the total dissipation is greater than the dissipation due to the poloidal velocity field $\boldsymbol{v}_P$ alone, and that all components in $\boldsymbol{v}_p=\partial_z\partial_x\phi\hat{\boldsymbol{x}}+\partial_z\partial_y\phi\hat{\boldsymbol{y}}-\Delta_2\phi\hat{\boldsymbol{z}}$ either obey Dirichlet conditions in z, or satisfy Neumann conditions and their integral over z is zero:

$$\begin{aligned}\sum_{ij}\langle\overline{(\partial_j v_i)^2}\rangle &\geqslant \sum_{ij}\langle\overline{(\partial_j v_{P,i})^2}\rangle\\ &\geqslant \langle\overline{(\partial_z v_{P,x})^2}+\overline{(\partial_z v_{P,y})^2}+\overline{(\partial_z v_{P,z})^2}\rangle\\ &\geqslant \pi^2\big(\langle\overline{v_{P,x}^2}\rangle+\langle\overline{v_{P,y}^2}\rangle+\langle\overline{v_{P,z}^2}\rangle\big).\end{aligned}\tag{36}$$

If H is an upper bound for $\mathrm{Nu}-1$, the poloidal energy is thus bounded as

$$\mathrm{Ra}H\geqslant 2\pi^2 E_{\mathrm{pol}}.\tag{37}$$

For infinite Pr, the velocity field is purely poloidal and poloidal and total energies are identical. For finite Pr, the toroidal field and a possible mean flow also contribute to the kinetic energy, but they do not appear in the constraints employed in the formulation of the optimization problem in Sec. IV. We therefore cannot obtain any additional information about the total energy, we can only hope to find tight bounds on the poloidal energy with the technique described above. The bound Eq. (37) derives solely from the energy budget Eq. (35) and the definitions of kinetic dissipation and energy. We expect to find tighter bounds by solving the full optimization problem.

Setting $Z=\langle\frac{1}{2}|\nabla\times\nabla\times(\phi\hat{\boldsymbol{z}})|^2\rangle$ and repeating the same computations as in the previous section yields bounds E on the poloidal energy. Figure 5 shows the bounds as a function of Ra for different cases and Table I summarizes the results by fitting power laws through the points at high Ra. A power-law fit is not quite satisfactory yet at infinite Pr for free-slip boundaries at the Ra accessed in these computations. Figure 6 presents for this reason an alternative point of view in which E is directly compared with $\mathrm{Ra}H$.

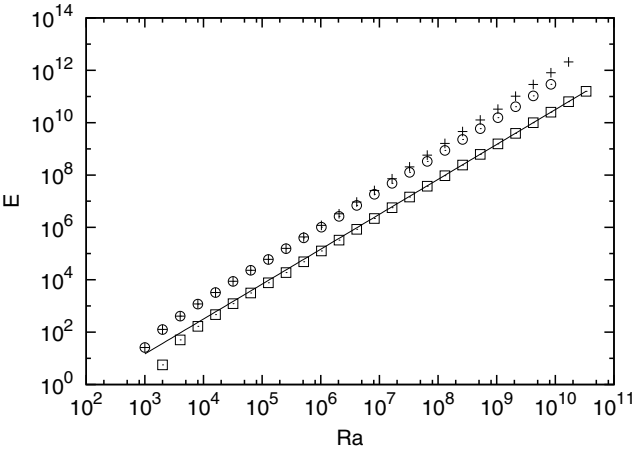

FIG. 5. The optimal upper bound E for the poloidal kinetic energy as a function of Ra at infinite Pr for stress free (circles) and no slip (squares) boundary conditions as well as for general Pr and free-slip boundaries (plus signs). The continuous line indicates the power law $0.00147\times\mathrm{Ra}^{4/3}$.

TABLE I. Fitted dependencies on Ra of H and E, the optimal upper bounds on Nu $-$ 1 and E_{pol}. The table also lists $\mathrm{Ra}H/(2\pi^2)$ for comparison with E.

	H	E	$\mathrm{Ra}H/(2\pi^2)$
Infinite Pr, free slip		$0.033 \times \mathrm{Ra}H$	$0.05066 \times \mathrm{Ra}H$
Infinite Pr, no slip	$0.139 \times \mathrm{Ra}^{1/3}$	$0.00147 \times \mathrm{Ra}^{4/3}$	$0.00704 \times \mathrm{Ra}^{4/3}$
General Pr, free slip	$0.055 \times \mathrm{Ra}^{1/2}$	$0.00106 \times \mathrm{Ra}^{3/2}$	$0.002786 \times \mathrm{Ra}^{3/2}$

In all cases, the full optimization problem improves prefactors compared with the direct estimate $\mathrm{Ra}H/(2\pi^2)$, but not the exponent in the power laws or the functional form of the Rayleigh number dependence. The prefactor improves by a factor ranging from 1.5 to 4.8.

There is an interesting curiosity about the bounds for free-slip boundaries. The bounds for infinite and general Pr agree to better than within 1% as long as there is only one wave number in the active set. The difference between the two cases becomes obvious only once the active set contains more than one wave number.

Some of the fitted power laws in Table I can be compared with data from direct numerical simulations. The comparison is scarce in the case of infinite Pr and no slip boundaries. Numerical simulations did not go to high enough Rayleigh numbers to be definitive about asymptotic scalings. Travis *et al.* [20] found $\mathrm{Nu} = 0.406 \times \mathrm{Ra}^{0.284}$, but Sotin and Labrosse [21] argue that this scaling only holds for time-independent convection and that $\mathrm{Nu} = 0.517 \times \mathrm{Ra}^{0.269}$ once time dependence sets in. However, their simulations were restricted to $\mathrm{Ra} < 10^7$. Theoretical arguments put forward by Grossmann and Lohse [22] lead to $\mathrm{Nu} \propto \mathrm{Ra}^{1/3}$ and $E_{\mathrm{pol}} \propto \mathrm{Ra}^{4/3}$. These exponents are the same as those listed in Table I for the bounds.

More results are available for infinite Pr and free-slip boundaries. In that case, Christensen [23] finds numerically $\mathrm{Nu} = 0.196 \times \mathrm{Ra}^{1/3}$ and Pandey *et al.* [24] obtain $\mathrm{Nu} = 0.23 \times \mathrm{Ra}^{0.32}$. These relations depend to some extent on the interval of Ra included in the fit (typically 10^5–10^8 for Ref. [24] and up to 10^{11} for Ref. [23]) and also the aspect ratio of the computational volume (which was actually 2D in Christensen's case), but the point is that there is roughly a factor of up to 2 between the bound H and the numerical results for $\mathrm{Ra} < 10^{10}$ with a widening gap if the quoted exponents persist to higher Ra. Pandey *et al.* [24] also give the kinetic energy for free-slip boundaries

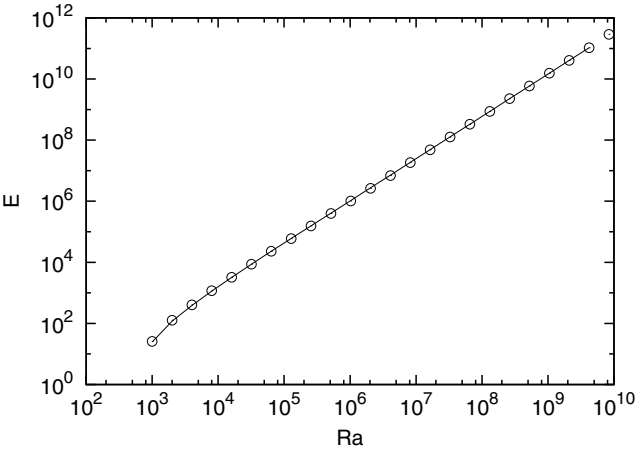

FIG. 6. The optimal upper bound E for the poloidal kinetic energy as a function of Ra at infinite Pr and stress free boundaries. The continuous line shows the function $0.033 \times \mathrm{Ra}H$, where H is the upper bound on the advective heat transport from Fig. 1.

at infinite Pr in a box of size $2\sqrt{(2)} : 2\sqrt{(2)} : 1$ as $0.02 \times \mathrm{Ra}^{6/5}$ for $10^5 \leqslant \mathrm{Ra} \leqslant 10^8$. This is nearly two orders of magnitude below the bound even at $\mathrm{Ra} = 10^8$, and the discrepancy is worsening with increasing Ra due to the discrepancy in the exponents. The kinetic energy deduced from the characteristic surface velocity obtained by Jarvis and Peltier [25] varies as $\mathrm{Ra}^{1.29}$. While closer to 1.4, this exponent is still much smaller than the one appearing in the bound.

At finite Pr, various simulations have found kinetic energy approximately proportional to Ra, so that in an all cases, the bounds for E_{pol} severely overestimate the kinetic energy.

Another apparent overestimate is the bound for Nu at general Pr. There are arguments [26] in favor of a scaling in the form $\mathrm{Nu} \propto \mathrm{Ra}^{1/2}$ at large Ra, the so-called ultimate regime. However, there is as of yet no unequivocal experimental or numerical observation of the ultimate regime and the exponents γ in $\mathrm{Nu} \propto \mathrm{Ra}^{\gamma}$ obtained from fits to observational data are less than $1/2$. Their precise value depends [27] on Pr and Ra, but γ is often found to be around $1/3$. The fact that no bound better than $\mathrm{Nu} - 1 = c\mathrm{Ra}^{1/2}$ with some constant c is known for 3D convection is sometimes seen as an indication that the ultimate regime will eventually be observed at high enough Ra.

A simple argument in favor of $\mathrm{Nu} \propto \mathrm{Ra}^{1/2}$ is dimensional analysis. This scaling must hold if the heat transport is independent of molecular diffusivities. If one applies the same argument to kinetic energy, one concludes that $g\alpha\Delta T h$ is the only acceptable combination of problem parameters other than molecular diffusivities with dimensions of velocity squared, which translates into a kinetic energy proportional to Ra. It is therefore very likely that the scaling in $\mathrm{Ra}^{3/2}$ shown by the bound will never be observed for the poloidal kinetic energy, not even in a surmised ultimate regime.

A scenario which generates large upper bounds is the existence of a stationary solution with high kinetic energy which is unstable and therefore never observed in an actual time evolution of the flow, but which prevents any bound from approaching the observed kinetic energy of the flow. It is at present not possible to tell whether this scenario is realized. The optimal flow field of the SDP is not a candidate for this possible stationary flow field. The optimal flow field contains only a few wave numbers and not their harmonics or other mixtures, as a solution of the Navier-Stokes equation would necessarily do.

Finally, while it is not possible to bound the energy contained in the nonpoloidal components, it is possible to bound the dissipation due to them, D_{np}. Again, the energy budget immediately provides us with a bound:

$$D_{\mathrm{np}} \leqslant \sum_{ij} \langle \overline{(\partial_j v_i)^2} \rangle = \mathrm{Ra}(\mathrm{Nu} - 1) \leqslant \mathrm{Ra}H. \tag{38}$$

With the data in Table I, we conclude that $D_{\mathrm{np}} \leqslant 0.055 \times \mathrm{Ra}^{3/2}$. Setting $Z = D_{\mathrm{np}}$ and going through the whole optimization procedure leads to a better bound, $D_{\mathrm{np}} \leqslant 0.021 \times \mathrm{Ra}^{3/2}$, shown in Fig. 7, but the improvement is once again only in the prefactor, not in the exponent.

In an effort to improve any of these bounds, one may think of having recourse of the maximum principle, which guarantees that, possibly after transients due to initial conditions, the temperature anywhere in the fluid must lie in between the temperatures of top and bottom boundaries, $0 \leqslant T = \theta + 1 - z \leqslant 1$. This means that the inequality Eq. (14) does not need to hold for any θ satisfying the boundary conditions, it is enough if it holds for every θ satisfying the boundary conditions and the maximum principle.

The inequality Eq. (19) decouples in k. It contains only quadratic terms for $k \neq 0$. To violate this inequality in one of the matrix blocks with $k \neq 0$, it is necessary that some block possesses at least one negative eigenvalue. This condition is independent of whether the admitted fields θ obey the maximum principle or not. For $k = 0$ on the other hand, the inequality Eq. (19) or (14) also contains linear terms and there is a non zero θ which minimizes the left hand side of Eq. (14). The minimizing θ was computed for the optimal λ's and was found to conform to the maximum principle in all cases. It would therefore lead to no improvement to explicitly impose this condition during the optimization process.

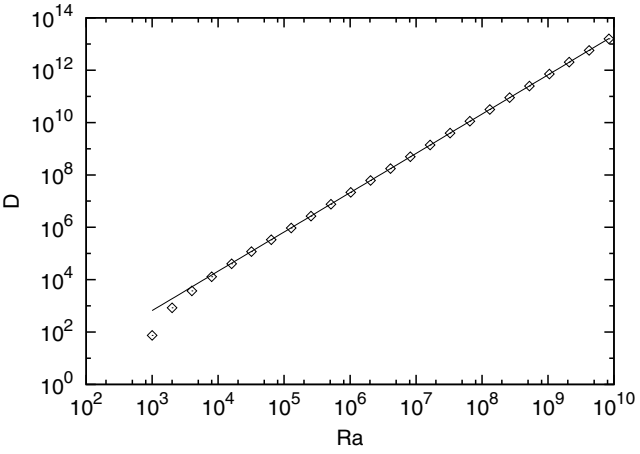

FIG. 7. The optimal upper bound D for the nonpoloidal dissipation D_{np} a function of Ra for general Pr and stress free boundaries. The continuous line indicates the power law $0.021 \times \mathrm{Ra}^{3/2}$.

VI. CONCLUSION

This paper presented a new method to numerically compute upper bounds for heat transport, dissipation, and poloidal energy in Rayleigh-Bénard convection both for infinite and general Prandtl number. The center piece of the method is a semidefinite program, which is numerically convenient to implement, but formally equivalent to the background field method.

The SDP can be solved with existing numerical libraries. While it is convenient to use an SDP solver as part of the overall procedure, it is not necessarily efficient. The obvious alternative is to solve Euler-Lagrange equations. The disadvantage of this option is that the Euler-Lagrange equations have many stationary points, only one of which is the solution of the SDP which is a convex optimization problem. On the other hand, finding optimal bounds amounts to finding a saddle point, with a minimization over the coefficients λ and a maximization over the wave numbers in the active set. These two optimizations have to be run separately and sequentially if an SDP solver based on central path methods is used, but both can be combined into a single root search if Euler-Lagrange equations are solved.

Once dissipation is bound, the mere definitions of dissipation and energy lead to a bound on energy. Including the additional constraints employed in optimum theory as it is used nowadays leads to tighter bounds, but only through improved prefactors, not through smaller exponents in power laws or new functional dependencies. It remains to be seen which additional constraints lead to further improvement of the upper bounds. The maximum principle for the temperature field can be of no help as it is already obeyed by the optimizing fields in the method presented here.

The exponent found for the bound on poloidal energy for general Prandtl numbers is not plausible for a tight bound. Either there exist stationary unstable flows which prevent better bounds, or the exponent can be improved by including additional constraints derived from the Navier-Stokes equations into the optimization process. If additional constraints have such an effect on the bound for the poloidal energy, they may also reduce the exponent of the known upper bound for the Nusselt number. This bound is compatible with the expected, but as of yet unobserved, ultimate regime of convection. The existence of this regime would be contradicted if the exponent in the bound for the Nusselt number could be reduced.

[1] E. Hopf, Ein allgemeiner Endlichkeitssatz der Hydrodynamik, Math. Ann. **117**, 764 (1941).
[2] W. Malkus, Outline for a theory for turbulent shear flow, J. Fluid Mech. **1**, 521 (1956).

[3] L. Howard, Heat transport by turbulent convection, J. Fluid Mech. **17**, 405 (1963).
[4] F. Busse, On Howard's upper bound for heat transport by turbulent convection, J. Fluid Mech. **37**, 457 (1969).
[5] C. R. Doering and P. Constantin, Energy Dissipation in Shear Driven Turbulence, Phys. Rev. Lett. **69**, 1648 (1992).
[6] C. R. Doering and P. Constantin, Variational bounds on energy dissipation in incompressible flows: III. Convection, Phys. Rev. E **53**, 5957 (1996).
[7] C. Seis, Scaling bounds on dissipation in turbulent flows, J. Fluid Mech. **777**, 591 (2015).
[8] G. Ierley, R. Kerswell, and C. Plasting, Infinite-Prandtl-number convection. Part 2. A singular limit of upper bound theory, J. Fluid Mech. **560**, 159 (2006).
[9] B. Wen, G. Chini, N. Dianati, and C. Doering, Computational approaches to aspect-ratio-dependent upper bounds and heat flux in porous medium convection, Phys. Lett. A **377**, 2931 (2013).
[10] B. Wen, G. P. Chini, R. R. Kerswell, and C. R. Doering, Time-stepping approach for solving upper-bound problems: Application to two-dimensional Rayleigh-Bénard convection, Phys. Rev. E **92**, 043012 (2015).
[11] G. Fantuzzi and A. Wynn, Optimal bounds with semidefinite programming: An application to stress-driven shear flows, Phys. Rev. E **93**, 043308 (2016).
[12] S. Boyd and L. Vandenberghe, *Convex Optimization* (Cambridge University Press, Cambridge, 2004).
[13] I. Tobasco, D. Goluskin, and C. Doering, Optimal bounds and extremal trajectories for time averages in dynamical systems, arXiv:1705.07096.
[14] D. Goluskin, Bounding averages rigorously using semidefinite programming: Mean moments of the Lorenz system, J. Nonlinear Sci. (2017), doi:10.1007/s00332-017-9421-2.
[15] J. Whithehead and C. Doering, Rigid bounds on heat transport by a fluid between slippery boundaries, J. Fluid Mech. **707**, 241 (2012).
[16] C. Nobili and F. Otto, Limitations of the background field method applied to Rayleigh-Bénard convection, J. Math. Phys. **58**, 093102 (2017).
[17] N. Vitanov, Upper bound on the heat transport in a horizontal fluid layer of infinite Prandtl number, Phys. Lett. A **248**, 338 (1998).
[18] N. Vitanov, On the optimum theory of turbulence, Doctoral thesis, University of Bayreuth, 1998.
[19] B. J. Schmitt and W. von Wahl, Decomposition of solenoidal fields into poloidal fields, toroidal fields and the mean flow. Applications to the Boussinesq-equations, in *The Navier-Stokes Equations II – Theory and Numerical Methods*, Lecture Notes in Mathematics, Vol. 1530, edited by J. G. Heywood, K. Masuda, R. Rautmann, and V. A. Solonnikov (Springer, Berlin, Heidelberg, 1992), pp. 291–305.
[20] B. Travis, P. Olson, and G. Schubert, The transition from two-dimensional to three-dimensional planforms in infinite Prandtl-number thermal convection, J. Fluid Mech. **216**, 71 (1990).
[21] C. Sotin and S. Labrosse, Three-dimensional thermal convection in an iso-viscous, infinite Prandtl number fluid heated from within and from below: Applications to the heat transfer of planetary mantles, Phys. Earth Planet. Inter. **112**, 171 (1999).
[22] S. Grossmann and D. Lohse, Thermal Convection at Large Prandtl Numbers, Phys. Rev. Lett. **86**, 3316 (2001).
[23] U. Christensen, The heat transport by convection rolls with free boundaries at high Rayleigh number, Geophys. Astrophys. Fluid Dyn. **46**, 93 (1989).
[24] A. Pandey, M. K. Verma, and P. K. Mishra, Scaling of heat flux and energy spectrum for very large Prandtl number convection, Phys. Rev. E **89**, 023006 (2014).
[25] G. Jarvis and W. Peltier, Mantle convection as a boundary layer phenomenon, Geophys. J. Roy. Astron. Soc. **68**, 389 (1982).
[26] R. Kraichnan, Turbulent thermal convection at arbitrary Prandtl number, Phys. Fluids **5**, 1374 (1962).
[27] G. Ahlers, S. Grossmann, and D. Lohse, Heat transfer and large-scale dynamics in turbulent Rayleigh-Bénard convection, Rev. Mod. Phys. **81**, 503 (2009).